Salt Bridges Destabilize a Leucine Zipper Designed for Maximized Ion Pairing between Helices†

Paul Phelan,‡,§ Alemayehu A. Gorfe,‡ Ilian Jelesarov,‡ Daniel N. Marti,‡ James Warwicker,|| and Hans Rudolf Bosshard*,‡

Biochemisches Institut der Universität Zürich, Winterthurerstrasse 190, CH-8057 Zürich, Switzerland, and University of Manchester Institute of Science and Technology, P.O. Box 88, Manchester M60 1QD, U.K.

Received October 11, 2001; Revised Manuscript Received December 10, 2001

ABSTRACT: Interhelical salt bridges are common in leucine zippers and are thought to stabilize the coiled coil conformation. Here we present a detailed thermodynamic investigation of the designed, disulfide-linked leucine zipper AB_{SS} whose high-resolution NMR structure shows six interhelical ion pairs between heptad positions *g* of one helix and *e′* of the other helix but no ion pairing within single helices. The average pK_a value of the Glu side chain carboxyl groups of AB_{SS} is slightly higher than the pK_a of a freely accessible Glu in an unfolded peptide [Marti, D. N., Jelesarov, I., and Bosshard, H. R. (2000) *Biochemistry 39,* 12804−12818]. This indicates that the salt bridges are destabilizing, a prediction we now have confirmed by determining the pH−stability profile of AB_{SS}. Circular dichroism-monitored unfolding by urea and by heating and differential scanning calorimetry show that the coiled coil conformation is ∼5 kJ/mol more stable when salt bridges are broken by protonation of the carboxyl side chains. Using guanidinium chloride as the denaturant, the increase in the free energy of unfolding on protonation of the carboxyl side chains is larger, ∼17 kJ/mol. The discrepancy between urea and guanidinium chloride unfolding can be ascribed to the ionic nature of guanidinium chloride, which screens charge−charge interactions. This work demonstrates the difficulty of predicting the energetic contribution of salt bridges from structural data alone even in a case where the ion pairs are seen in high-resolution NMR structures. The reason is that the contribution to stability results from a fine balance between energetically favorable Coulombic attractions and unfavorable desolvation of charges and conformational constraints of the residues involved in ion pairing. The apparent discrepancy between the results presented here and mutational studies indicating stabilization by salt bridges is discussed and resolved. An explanation is proposed for why interhelical salt bridges are frequently found in natural coiled coils despite evidence that they do not directly contribute to stability.

Salt bridges between oppositely charged side chains are frequently observed in high-resolution protein structures.[1] They often are assumed to stabilize the native protein conformation. However, careful experimental and computational analysis indicates that ionic interactions between oppositely charged protein side chains are not always stabilizing (*1*−*7*). The reason is that the net contribution to stability results from a delicate balance between energetically favorable Coulombic attraction on one hand and unfavorable desolvation energies and conformational constraints imposed by the salt bridge on the other hand. As a result, the electrostatic free energy contribution to protein stability does not correlate with the number of ion pairs in a protein, but rather depends on the exact location and geometrical constraints of the ion pairs. Some studies suggest that only a few ion pairs contribute favorably to protein stability, for example, when buried in the protein interior (*2*, *8*, *9*). Other studies argue that most salt bridges in monomeric proteins are stabilizing, regardless of their solvent accessibility (*4*). It is difficult to infer stabilizing or destabilizing electrostatic free energy contributions from structural data alone. One has to combine structural, equilibrium thermodynamic, and computational data on all the charges in the folded native protein as well as in the ensemble of denatured[2] polypeptide chains to differentiate between stabilizing and destabilizing ion pairs.

Coiled coils are helical dimerization motifs consisting of two α-helical peptides wound around each other to form a superhelix, which is held together by hydrophobic packing along the dimer interface (*10*, *11*). The structure originates from repetition of a seven-residue sequence motif, $(abcdefg)_n$.

† This work was supported in part by the Swiss National Science Foundation (Grant 31.55308.98) and by the Bundesamt für Bildung und Wissenschaft (Grant BBW 970592).

* To whom correspondence should be addressed. Telephone: +41 1 635 5540. Fax: +41 1 635 6805. E-mail: hrboss@bioc.unizh.ch.

‡ Biochemisches Institut der Universität Zürich.

§ Present address: Department of Chemistry, Merkert Chemistry Center, Boston College, Chestnut Hill, MA 02167.

|| University of Manchester Institute of Science and Technology.

[1] A salt bridge is defined as an electrostatic interaction between oppositely charged, ionized amino acid side chains.

[2] By denatured we mean any ensemble of non-native states induced by a chemical denaturant or by heat. The denatured state we distinguish from the unfolded state, which is the state with the highest solvent accessibility of all residues, theoretically the fully extended peptide chain.

10.1021/bi011920c CCC: $22.00
Published on Web 02/06/2002

Hydrophobic residues dominate at the *a* and *d* positions and interact at the dimer interface (*11*−*14*). While interhelical hydrophobic packing is the major source of stability, attractive and repulsive electrostatic interactions across the dimer interface can also contribute to the free energy of unfolding, ΔG_U[3] (*15*−*24*). Interhelical salt bridges originate from the close interhelical approach of side chains in the *g* position of one helix and the following *e′* position of the other helix ($i-i'+5$ pair, where the prime indicates the residue in the other helix) (*15*, *25*−*27*). Because of the 2-fold symmetry of the dimeric coiled coil, there are two ion pairs per heptad: *g*−*e′* and *g′*−*e* (Figure 1b). Electrostatic repulsion across the coiled coil interface opposes folding and controls the formation of homo- versus heterodimeric structures, as is well documented for the leucine zipper domain of the jun-fos transcription factor (*28*−*32*). While it is clear that repulsive interactions are destabilizing, the situation is more complex for attractive interactions between oppositely charged side chains across the dimer interface. Published results are ambiguous (*24*, *33*−*37*).

We reasoned that a heterodimeric coiled coil composed of an acidic peptide chain with Glu in all its *e* and *g* positions, and of a basic peptide chain with Lys or Arg in all its *e′* and *g′* positions, should offer an excellent model for investigating the energetic contribution of interhelical salt bridges to coiled coil stability. Such coiled coil heterodimers are forming a kind of molecular "Velcro" (*18*) and have been designed before by us (*22*, *38*) and by others (*17*−*21*, *39*, *40*). Our model is the disulfide-linked heterodimer AB_{SS} (*33*) in which a maximum of seven interhelical *g*−*e′* salt bridges can be formed (Figure 1). Six salt bridges[4] have been confirmed by high-resolution NMR spectroscopy of AB_{SS} (Figure 1c and Table 1). The mean pK_a of all side chain carboxyl groups of AB_{SS} is 4.47 ± 0.26 (Table 1). This is slightly higher than the pK_a of ∼4.2−4.4 for a freely accessible Glu side chain in an unfolded peptide (*34*, *41*−*43*). Hence, on average, the salt bridges seem to destabilize the coiled coil conformation, and breaking salt bridges through protonation of the Glu side chains should increase the stability of AB_{SS} (*34*, *35*, *44*). This we now have confirmed by chemical and thermal unfolding experiments in the pH range of 2−8.

MATERIALS AND METHODS

Materials

Peptides. Peptides A and B and their disulfide-linked dimer were chemically synthesized and purified as described previously (*33*). GdmCl and urea were of the highest purity available from Fluka. Peptide concentrations were determined by UV absorbance in 6 M GdmCl, with an $\epsilon_{275.3}$ of 1450 M^{-1} cm^{-1} (*45*, *46*).

Buffers. All experiments were conducted in a standard buffer with an ionic strength of 0.1 M. The buffer was composed of phosphoric, citric, and boric acid (7.5 mM each) adjusted to the desired pH with KOH or HCl and to an ionic strength of 0.1 M with KCl. The pH of buffers containing urea or GdmCl was adjusted after adding the denaturant. The pH of this buffer changes only very slightly with temperature and was not corrected for.

Methods

CD Spectroscopy. CD measurements were performed on a Jasco-715 spectropolarimeter equipped with a computer-controlled water bath, using thermostated cuvettes with a 1 or 10 mm path length. Thermal unfolding curves were measured by continuously recording the ellipticity at 222 nm and with data collection every 20 s. Reversibility was checked by two cycles of heating and cooling. Altogether, 66 experiments were performed under 66 different experimental conditions at 0.5 pH unit intervals in the pH range of 2−7 and in the absence or presence of small, nondenaturing amounts of either GdmCl (0−2.75 M) or urea (0−3 M). With few exceptions, each thermal unfolding experiment was performed four times.[5]

Unfolding by urea or GdmCl at fixed temperature was monitored at 222 nm. Data were sampled for 3 min at 25 °C after incubation of the peptide for 12−15 h at the desired denaturant concentration. Urea and GdmCl unfolding experiments were performed between pH 2 and 8 at intervals of 0.5 pH unit.[6]

Analysis of CD Data. Analysis of heat and denaturant-induced unfolding curves followed the formulation describing a two-state transition between the folded and the unfolded state. The unfolding constant is defined as

$$K_U = f_U/(1 - f_U) \quad (1)$$

where f_U is the fraction of unfolded peptide. At each temperature or denaturant concentration, the observed molar ellipticity per residue of the folded and the unfolded state is

$$[\theta] = f_U[\theta_U] + (1 - f_U)[\theta_F] \quad (2)$$

where $[\theta_U]$ and $[\theta_F]$ are the molar ellipticity per residue of the unfolded and folded protein, respectively. $[\theta_U]$ and $[\theta_F]$ were assumed to be linear functions of temperature or denaturant concentration of the general form $[\theta_i] = [\theta_{i,0}] + \alpha_i T$ or $[\theta_i] = [\theta_{i,0}] + \alpha_i$[denaturant], with i indicating the U or F state. Combining eqs 1 and 2 gives

$$[\theta] = (K_U/(1 - K_U))([\theta_U] - [\theta_F]) + [\theta_F] \quad (3)$$

The slope α_F of the pre-transition baseline was obtained from a fit according to eq 3. The slope α_U of the post-transition baseline of the thermal unfolding curves was very small and was fixed at zero. The slope α_U of the post-transition baseline

[3] Abbreviations: CD, circular dichroism; DBM, denaturant binding model; DSC, differential scanning calorimetry; GdmCl, guanidinium chloride; HPLC, high-performance liquid chromatography; LEM, linear extrapolation model. Thermodynamic parameters: K_U, equilibrium constant of unfolding; T_m, midpoint of thermal transition; ΔC_p, heat capacity change of unfolding; ΔG_U, free energy change of unfolding; ΔH_U, enthalpy change of unfolding; ΔH_m, enthalpy change of unfolding at T_m.

[4] Residues are assumed to form a salt bridge if the average atom distance is ≤5 Å (Table 1), which is the case in the majority of the 25 NMR conformers shown in Figure 1c.

[5] Thermodynamic parameters obtained from thermal unfolding experiments are shown in Table 2 of the Supporting Information. The effect of small, nondenaturing amounts of urea and GdmCl on $\partial\Delta H_m/\partial$[denaturant] and $\partial T_m/\partial$[denaturant] is shown in Figure 1 and Table 1 of the Supporting Information.

[6] Thermodynamic parameters obtained from denaturant unfolding experiments are shown in Tables 3 and 4 of the Supporting Information.

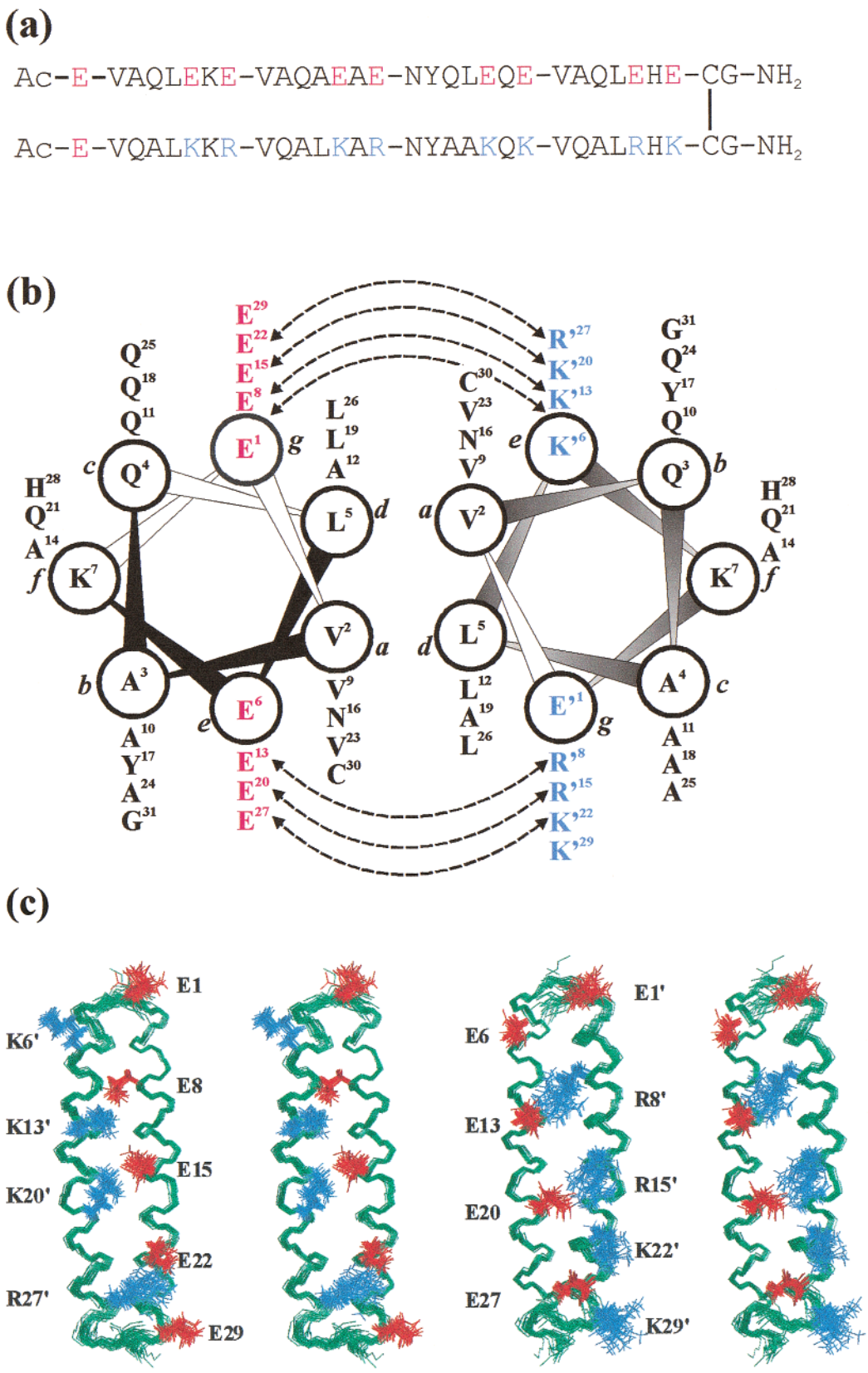

FIGURE 1: Primary sequence (a), helical-wheel representation (b), and NMR structures (c) of the heterodimeric leucine zipper AB_{SS}. (a) Amino acid sequence of the disulfide-linked acidic (top) and basic (bottom) peptides. Heptad sequence motifs are separated by dashes, and the disulfide bond is represented by a vertical line. Acidic and basic residues in the *e* and *g* positions are in red and blue, respectively. (b) Helical-wheel representation of the aligned acidic (left) and basic (right) helices. Heptad positions are denoted by italic lowercase letter. Interhelical ion pairs involving acidic (red) and basic (blue) residues in the *e*, *g*, *e*′, and *g*′ positions are highlighted with dashed arrows. (c) Alignment of charged residues in an ensemble of 25 selected AB_{SS} structures (*33*). Stereoviews of the spatial orientations of acidic (red) and basic (blue) residues in the *e*, *g*, *e*′, and *g*′ positions are shown for the "front view" (left stereopair) and the "back view" (right stereopair) of AB_{SS}. Only the side chains of acidic and basic residues are displayed. Backbone bonds are outlined in green. Panel c was reproduced from ref *33*.

Table 1: pK_a Values of Glutamic Acid Side Chains and Average Atom Distances of Ion Pairs in the Ensemble of 25 NMR Structures of Leucine Zipper AB_{SS} Shown in Figure 1c

residue	pK_a[a]	partner residue in ion pair	residue pair	average distance (Å)
Glu-1	4.14	Lys-6′	E^1 $O^{\epsilon1}$−$K^{6'}$ N^{ζ}	12.60 ± 1.00
			E^1 $O^{\epsilon2}$−$K^{6'}$ N^{ζ}	12.51 ± 1.11
Glu-1′	4.22	Glu-6[b]	$E^{1'}$ $O^{\epsilon1}$−E^6 $O^{\epsilon1}$	11.66 ± 0.99
			$E^{1'}$ $O^{\epsilon1}$−E^6 $O^{\epsilon2}$	11.93 ± 0.76
			$E^{1'}$ $O^{\epsilon2}$−E^6 $O^{\epsilon1}$	11.67 ± 1.10
			$E^{1'}$ $O^{\epsilon2}$−E^6 $O^{\epsilon2}$	11.98 ± 0.98
Glu-6	4.82	Glu-1′ [b]		
Glu-8[c]	4.52	Lys-13′	E^8 $O^{\epsilon1}$−$K^{13'}$ N^{ζ}	4.01 ± 0.88
			E^8 $O^{\epsilon2}$−$K^{13'}$ N^{ζ}	3.83 ± 0.82
Glu-13[c]	4.37	Arg-8′	E^{13} $O^{\epsilon1}$−$R^{8'}$ $N^{\eta1}$	5.50 ± 0.78
			E^{13} $O^{\epsilon2}$−$R^{8'}$ $N^{\eta1}$	5.55 ± 0.85
			E^{13} $O^{\epsilon1}$−$R^{8'}$ $N^{\eta2}$	3.68 ± 0.79
			E^{13} $O^{\epsilon2}$−$R^{8'}$ $N^{\eta2}$	3.67 ± 0.96
			E^{13} $O^{\epsilon1}$−$R^{8'}$ N^{ϵ}	4.81 ± 0.75
			E^{13} $O^{\epsilon2}$−$R^{8'}$ N^{ϵ}	4.83 ± 0.98
Glu-15[c]	4.11	Lys-20′	E^{15} $O^{\epsilon1}$−$K^{20'}$ N^{ζ}	3.82 ± 0.73
			E^{15} $O^{\epsilon2}$−$K^{20'}$ N^{ζ}	3.72 ± 0.86
Glu-20[c]	4.41	Arg-15′	E^{20} $O^{\epsilon1}$−$R^{15'}$ $N^{\eta1}$	5.33 ± 0.94
			E^{20} $O^{\epsilon2}$−$R^{15'}$ $N^{\eta1}$	5.23 ± 0.93
			E^{20} $O^{\epsilon1}$−$R^{15'}$ $N^{\eta2}$	4.07 ± 1.31
			E^{20} $O^{\epsilon2}$−$R^{15'}$ $N^{\eta2}$	4.05 ± 1.28
			E^{20} $O^{\epsilon1}$−$R^{15'}$ N^{ϵ}	4.92 ± 1.15
			E^{20} $O^{\epsilon2}$−$R^{15'}$ N^{ϵ}	4.75 ± 1.18
Glu-22[c]	4.82	Arg-27′	E^{22} $O^{\epsilon1}$−$R^{27'}$ $N^{\eta1}$	5.21 ± 1.17
			E^{22} $O^{\epsilon2}$−$R^{27'}$ $N^{\eta1}$	4.97 ± 1.09
			E^{22} $O^{\epsilon1}$−$R^{27'}$ $N^{\eta2}$	4.55 ± 1.17
			E^{22} $O^{\epsilon2}$−$R^{27'}$ $N^{\eta2}$	4.35 ± 1.05
			E^{22} $O^{\epsilon1}$−$R^{27'}$ N^{ϵ}	4.93 ± 0.97
			E^{22} $O^{\epsilon2}$−$R^{27'}$ N^{ϵ}	4.62 ± 0.79
Glu-27[c]	4.65	Lys-22′	E^{27} $O^{\epsilon1}$−$K^{22'}$ N^{ζ}	4.87 ± 1.46
			E^{27} $O^{\epsilon2}$−$K^{22'}$ N^{ζ}	5.02 ± 1.49
Glu-29	4.63	none		

[a] pK_a of the Glu side chain carboxyl group, from ref *33*; the mean pK_a for all 10 Glu residues is 4.47 ± 0.26. [b] Charge−charge repulsion. [c] These residues are involved in salt bridges,[3] and their mean pK_a is 4.48 ± 0.25.

of the denaturant unfolding curves was obtained from the fits with eq 3.

Analysis of Thermal Unfolding Curves. To obtain the unfolding enthalpy at the melting temperature T_m, the data were analyzed by fitting $[\theta]_{222}$ to eq 3 with K_U being equal to $\exp[(\Delta H_U/R)(1/T_m - 1/T)]$. The fits provided values of ΔH_U, T_m, and α_F. In addition, the van't Hoff enthalpy change, ΔH_U^{vH}, was obtained from the slope of a plot of $-R \ln K_U$ versus $1/T$, using only $[\theta]_{222}$ values in the narrow range of $T_m \pm 3$ °C where ΔH_U is assumed to be independent of T. Values of ΔH_U from the fit according to eq 3 and of ΔH_U^{vH} from the van't Hoff plot were identical within the error of the fitting.

The unfolding heat capacity change, ΔC_p, was calculated by global analysis of all melting curves recorded between pH 2 and 6 with the help of the following equation derived from the Gibbs−Helmholtz relationship:

$$\ln K_U = \left[-\frac{\Delta H_U(T_R,\mathrm{pH})}{R} + \frac{\Delta C_p T_R}{R}\right]\left[\frac{1}{T} - \frac{1}{T_m(\mathrm{pH})}\right] + \frac{\Delta C_p}{R}\ln\frac{T_R}{T_m(\mathrm{pH})} \quad (4)$$

K_U is the unfolding constant obtained from the melting trace. The fitting parameters are ΔC_p, the unfolding enthalpy change $\Delta H_U(T_R,\mathrm{pH})$, and the midpoint temperature $T_m(\mathrm{pH})$ at a given pH and at an arbitrary reference temperature T_R (298 K was used).

Analysis of Denaturant Unfolding Curves. To obtain the unfolding free energy extrapolated to zero denaturant concentration, ΔG_U^w, three different fitting procedures were used. First, the data were analyzed by fitting $[\theta]_{222}$ to eq 3 using

$$K_U = \exp[(m[\mathrm{D}] - \Delta G_U^{\,w})/RT] \quad (5)$$

where [D] is the denaturant concentration and m is the change of ΔG with [D] assuming the linear extrapolation model (LEM) (*47*). The fits provided values of ΔG_U^w, m, and the pre- and post-transition baselines α_F and α_U, respectively. Since the statistical significance of the fitted parameters was low, a more robust estimate was obtained by using eq 6:

$$K_U = \exp[-m([\mathrm{D}] - [\mathrm{D}]_{0.5})/RT] \quad (6)$$

where $[D]_{0.5}$ is the denaturant concentration at the midpoint of the transition. ΔG_U^w was calculated from $m[D]_{0.5}$. Finally, the entire set of denaturant unfolding traces was simultaneously fit according to the denaturant binding model (DBM) (*48*):

$$\Delta G = \Delta G_U^{\,w} - RT \ln(1 + ak)^{\Delta n} \quad (7)$$

where k is the denaturant binding constant, a is the activity of the denaturant solution, and Δn is the difference in the number of denaturant binding sites between the folded and denatured protein. The values of k and a were taken from ref *49*. The fits provided ΔG_U^w and Δn values. Values of ΔG_U^w deduced from the LEM and the DBM, respectively, were very similar.

Differential Scanning Calorimetry. DSC experiments were performed on the VP-DSC microcalorimeter (MicroCal Inc.). The peptide was dialyzed for 18−20 h against the same buffer used to establish the baseline. The scan rate was 1 °C/min. Reversibility was checked by two to four cycles of heating and cooling and was better than 95%. Calorimetric and van't Hoff unfolding enthalpies, ΔH_U^{cal} and ΔH_U^{vH}, respectively, were calculated from the calorimetric traces as described previously (*50*).

Error Estimates. The 95% confidence limit of the fits to the experimental data is shown, unless indicated otherwise.

Computational Methods. The pH−stability data represented as a dashed line in Figure 6b were calculated by solving the pH derivative of the electrostatic free energy of unfolding from the mean fractional charge difference between the denatured (q_D) and native (q_N) states:

$$\delta\Delta G/\delta\mathrm{pH} = 2.303RT(q_D - q_N) \quad (8)$$

For calculating the full electrostatic energy, q_N was computed from the experimental pK_a values (*33*) and q_D was obtained from pK_a values calculated for a sequence-based extended model of the denatured state (*51*).

The effect of charge−charge interactions on the pH−stability profile (continuous line in Figure 7) was calculated with the help of pK_a values calculated for the native and denatured states and setting the desolvation and background interaction terms to zero (*5*). Native state pK_a values were

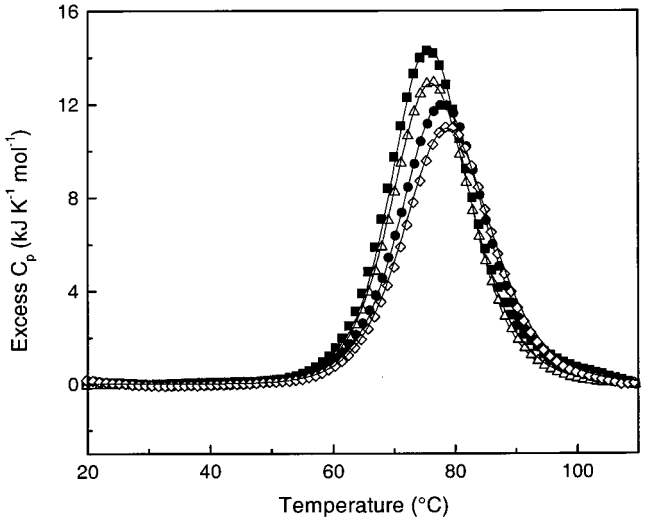

FIGURE 2: Excess heat capacity traces for the melting of AB_{SS} at pH 2, 3, 4, and 5 (from left to right) measured by differential scanning calorimetry. The solid lines are best fits describing two-state folding.

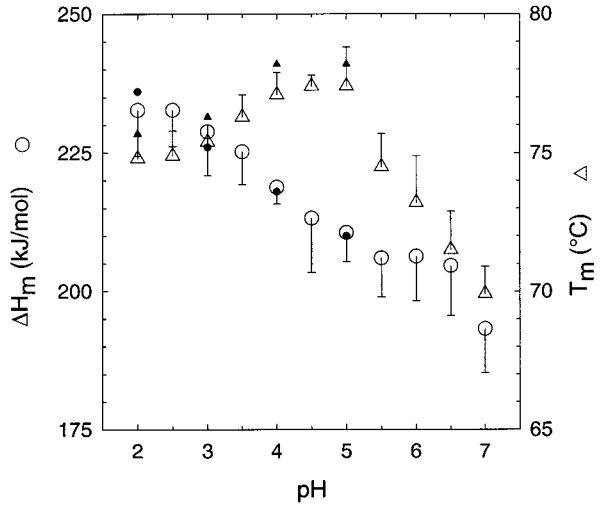

FIGURE 3: Change of ΔH_m (circles, left ordinate) and T_m (triangles, right ordinate) with pH. T_m and ΔH_m were obtained from thermal unfolding followed by CD (large symbols). Error bars indicate the standard error of the mean from two to six single experiments. T_m and ΔH_{cal} obtained from DSC (small symbols) are from single experiments, results of which are shown in Figure 2.

calculated with the help of an averaging cluster-based protocol applied to MD-generated ensembles of AB_{SS} (*52*). pK_a values of the denatured state were calculated assuming a fully extended chain (*53*). Calculations were carried out with the MEAD program suite (*54*, *55*) using PARSE charges and radii (*56*), a 1.4 Å probe radius, a 2 Å Stern layer, an ionic strength of 0.1, and dielectric constants of 4 and 80 for the protein and the bulk solvent, respectively.

RESULTS

Peptide Structure. Leucine zipper AB_{SS} is composed of an acidic A-chain and a basic B-chain connected by a disulfide bridge near the C-terminus. The sequences of the two peptide chains are shown in Figure 1a. The *e* and *g* heptad positions of the A-chain are occupied by Glu and those of the B-chain by Lys or Arg. These residues may form seven attractive interhelical interactions in the coiled coil conformation as shown by the helical-wheel representation in Figure 1b. In designing AB_{SS}, we purposely omitted intrahelical attractive $i + 3$ and $i + 4$ ion pairs (*57*) to focus on interhelical salt bridges. Six of the seven potential salt bridges are seen in most of the NMR structures (Figure 1c, Table 1, and ref *33*).[4] There is no salt bridge between Glu-1 and Lys-6′, possibly because the coiled coil conformation is less compact near the N-termini (*33*). One repulsive interaction was expected between Glu-1 and Glu-6′ and verified by an 11 Å distance between these side chains (Table 1). The CD spectrum of folded AB_{SS} shows the typical features of a coiled coil with minima at 208 and 222 nm (not shown). The structure is stable in the pH range of 2−8 (*33*), which has allowed the investigation of the pH dependence of stability without complications from acid denaturation.

Thermal Unfolding. Thermal unfolding was followed from the increase with temperature of the molar ellipticity at 222 nm (Figure 2 of ref *33*). Unfolding was >95% reversible up to pH 6. At higher pH values, reversibility dropped to 70−80%. DSC experiments were performed at pH 2, 3, 4, and 5 and were >95% reversible (Figure 2). The enthalpy of unfolding decreases, and T_m increases when the pH is increased from 2 to 5, as also described for another acid and base coiled coil heterodimer (*58*). The van't Hoff enthalpy, ΔH^{vtH}, calculated from the melting traces assuming a two-state transition, and the model-independent calorimetric enthalpy given by the integral of the melting transition, ΔH^{cal}, are identical within error. This is a very strong argument for the folding reaction of AB_{SS} being two-state, as observed for many other leucine zippers.

Figure 3 shows values of the melting temperature and the corresponding enthalpy change, versus pH. ΔH_m decreases with increasing pH, while T_m peaks at pH 4.5. The change of ΔH_m with temperature is very small and apparently does not correlate linearly with T_m, as reported for another model zipper featuring many inter- and intrahelical ion pairs (*58*). To estimate ΔC_p from the slope of a plot of ΔH_m versus T_m, the range of T_m and ΔH_m values had to be increased. To this end, thermal unfolding experiments were repeated in the presence of small, nondenaturing amounts of GdmCl or urea. The pre- and post-transition slopes and the shape of the unfolding transition were the same in the presence and absence of small amounts of denaturant. Also, plots of T_m or ΔH_m versus the concentration of GdmCl or urea, respectively, were linear (Figure 1 of the Supporting Information). This verifies that the mechanism of thermal unfolding was not changed by the denaturant and that, therefore, addition of small amounts of denaturant is a valid procedure for enlarging the range of T_m and ΔH_m.

Figure 4 shows a van't Hoff plot of the data obtained in the presence of nondenaturing amounts of GdmCl and urea. Within experimental scatter, ΔH_m changes linearly with T_m. The heat capacity change (ΔC_p) of unfolding calculated from the slope of the plot is 2.5 ± 0.4 kJ mol^{-1} K^{-1}. This value agrees with a ΔC_p of 2.2 ± 0.1 mol/K obtained from globally fitting the melting traces between pH 2 and 6 with the help of eq 4. Furthermore, we have calculated a ΔC_p 2.1 mol/K from the NMR structure (*33*). Because the ΔC_p of 2.5 kJ mol^{-1} K^{-1} (Figure 4) is based on the largest range of T_m values, this value was used to calculate the pH−stability profile at 25 °C [Figure 6 (▲)]. We note that ΔC_p seems to slightly increase with increasing pH, but the increase is not

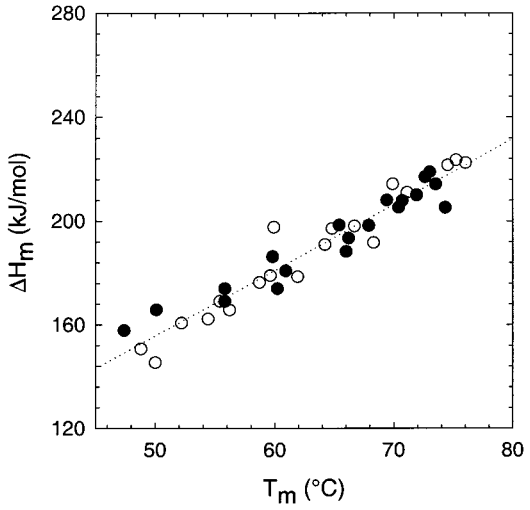

FIGURE 4: Kirchhoff analysis of thermal unfolding data measured in the presence of nondenaturing amounts of urea or GdmCl. The slope of the linear best fit to all data points yields a ΔC_p of 2.5 ± 0.4 kJ mol^{-1} K^{-1}. Data collected in the pH range of 2−3 (filled symbols) yield a ΔC_p of 2.2 ± 0.5 kJ mol^{-1} K^{-1}, and data in the pH range of 4−6 (empty symbols) yield a ΔC_p of 2.8 ± 0.5 kJ mol^{-1} K^{-1}.

statistically significant (see the legend of Figure 4).

Denaturant Unfolding. Figure 5 shows representative GdmCl and urea unfolding curves determined at pH 2 and 7, respectively. LEM and DBM analyses of denaturant unfolding (eqs 5−7) yield very similar results, supporting the applicability of the linear extrapolation method. The *m* values of the LEM analyses (eqs 5 and 6) are pH-independent (Figure 5c). The difference in denaturant binding sites between folded and unfolded AB_{SS} in the DBM (Δn of eq 7) is 10 for GdmCl and 75 for urea, in agreement with similar values reported for other small proteins when expressed on a per residue basis (*49*).

The molar ellipticity $[\theta]_{222}$ of the folded coiled coil measured in the absence of the denaturant was more negative at pH 2 than at pH 7 (Figure 5). A higher "helical content" at low pH has been observed previously (*33*). If the two disulfide-linked 31-residue peptide chains of AB_{SS} are treated as a single, 62-residue α-helix, one calculates a $[\theta]_{222}$ of −36000 deg cm^2 dmol^{-1} (*59*), only slightly higher than the observed molar ellipticities.

pH−Stability Profiles from Unfolding by Denaturant and Heat. Plotting the values of ΔG_U against pH yields the pH−stability profiles shown in Figure 6a. This plot demonstrates increasing stability with decreasing pH. However, the stability differences deduced by urea and GdmCl unfolding do not match. The stability difference between pH 2 and 7 is ∼5 kJ/mol for urea unfolding and ∼17 kJ/mol for GdmCl unfolding.

One can also calculate a pH−stability profile from the thermal unfolding data using eq 9.

$$\Delta G_U = \Delta H_m(1 - T/T_m) + \Delta C_p[T - T_m - T\ln(T/T_m)] \quad (9)$$

The equation is based on the assumption that ΔC_p does not change with pH and temperature. The calculation was performed using the values of ΔH_m and T_m measured in the absence of denaturant (Figure 3) and a pH-independent ΔC_p of 2.5 kJ mol^{-1} K^{-1}. ΔG_U thus calculated may have a larger

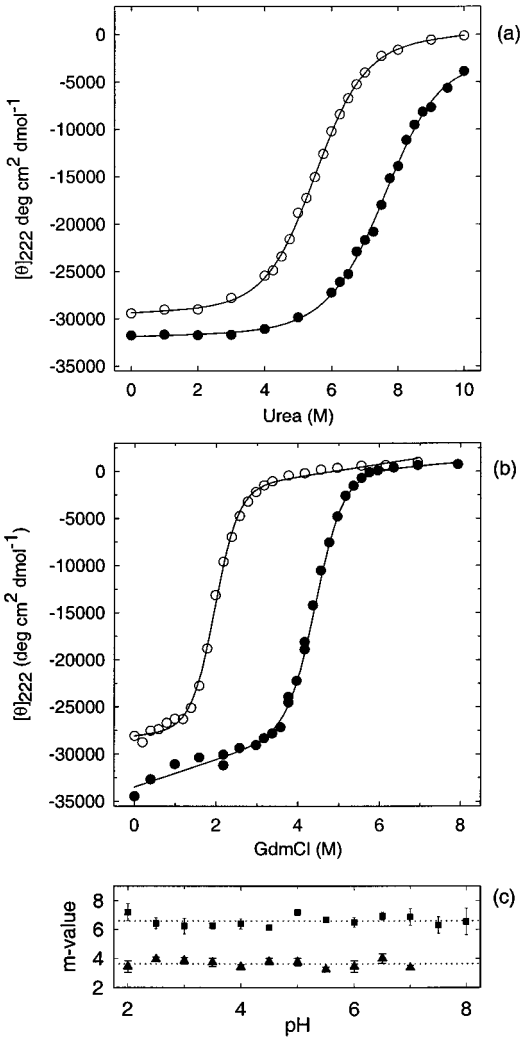

FIGURE 5: Denaturant unfolding curves presented as the change in molar ellipticity at 222 nm vs denaturant concentration. (a) Unfolding induced by urea at pH 2 (filled symbols) and pH 7 (empty symbols). (b) Unfolding induced by GdmCl at pH 2 (filled symbols) and pH 7 (empty symbols). The larger difference at 0 M denaturant between the pH 2 and 7 traces in panel b, as compared to panel a, is attributed to experimental error in determining protein concentration, which is the largest single source of error of $[\theta]_{222}$. (c) Slopes *m* from LEM analysis of urea unfolding curves (■) and GdmCl unfolding curves (▲) measured at different pH values. The mean *m* values are 6.59 ± 0.36 kJ mol^{-1} M^{-1} for urea unfolding and 3.64 ± 0.26 kJ mol^{-1} M^{-1} for GdmCl unfolding.

error than ΔG_U from denaturant unfolding because of the extrapolation from T_m to 25 °C. Still, the extrapolated thermal ΔG_U follows approximately the pH dependence of ΔG_U from urea unfolding (compare ■ and ▲ in Figure 6a). Even if we assume that ΔC_p is pH-dependent and changes linearly from 2 kJ mol^{-1} K^{-1} at pH 2 to 3 kJ mol^{-1} K^{-1} at pH 7, the thermal ΔG_U would decrease by only 8 kJ/mol from pH 2 to 7, much smaller than the change of 17 kJ/mol deduced from GdmCl unfolding.

Increasing Stability at Acidic pH Follows from Lower pK_a Values of Glu Side Chains in the Unfolded Protein. The difference in stability between acidic and neutral pH, that is, between AB_{SS} with uncharged and charged Glu side chains, respectively, is best seen in a plot of $\Delta\Delta G_U$ against pH (Figure 6b). $\Delta\Delta G_U$ is the free energy of unfolding normalized to a ΔG_U of 0 at pH 2. The difference in the pK_a of an ionizable residue measured in the denatured and folded

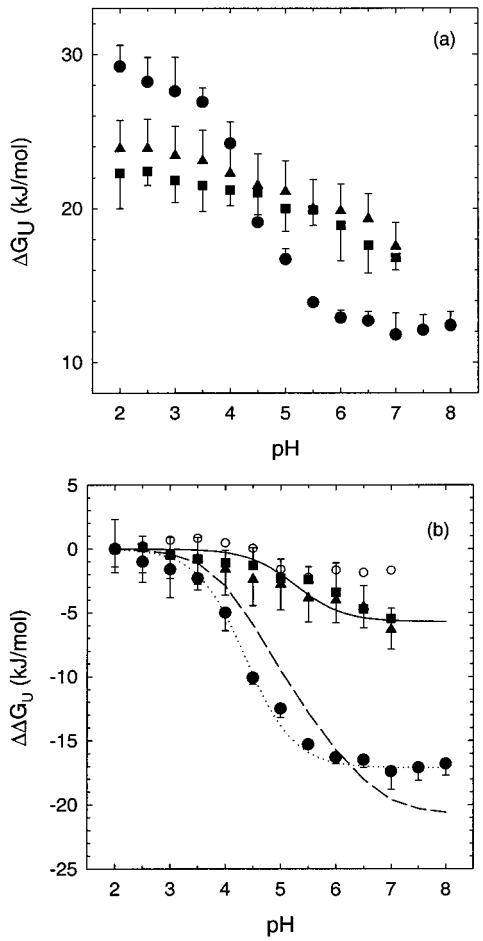

FIGURE 6: pH−stability profile of coiled coil AB_{SS} presented as the change in the free energy of unfolding vs pH. (a) Absolute free energy change of unfolding, ΔG_U, vs pH. (b) Relative free energy change of unfolding ($\Delta\Delta G_U$) defined as ΔG_U(pH) − ΔG_U(pH 2) vs pH: (●) ΔG_U from GdmCl unfolding experiments, (■) ΔG_U from urea unfolding experiments, and (▲) ΔG_U at 25 °C extrapolated from thermal unfolding experiments (eq 9) using the values of ΔH_m and T_m from Figure 3 and a ΔC_p of 2.5 kJ mol^{-1} K^{-1}. (b) Calculated pH−stability curves. The empty symbols were calculated from the data in Figure 3 with the help of eqs 12 and 13. The solid line was calculated assuming a mean pK_a for the 10 Glu side chains of 4.47 in folded AB_{SS} and of 4.37 in urea- and heat-denatured AB_{SS}. The dotted line was calculated assuming a mean pK_a for the 10 Glu side chains of 4.47 in folded AB_{SS} and of 4.17 in GdmCl-denatured AB_{SS}. The dashed line was calculated on the basis of the experimental pK_a values of folded AB_{SS} (*33*) and on the basis of the calculated pK_a values for a sequence-based extended model of the denatured state (*51*). See Materials and Methods for details of the calculations.

protein reflects the difference in the contribution to protein stability of the residue in the charged and uncharged form, respectively (*34*, *44*). The influence of the protonation state of a particular Glu side chain on $\Delta\Delta G_U$ is

$$\Delta\Delta G_U = \Delta G_{U^-} - \Delta G_{U0} \quad (10)$$

where ΔG_{U^-} refers to the charged form and ΔG_{U0} to the uncharged form of the side chain. $\Delta\Delta G_U$ can be expressed as

$$\Delta\Delta G_U = -2.303RT(pK_a^F - pK_a^D) \quad (11)$$

where D and F refer to the denatured and folded protein, respectively. Figure 6b shows that $\Delta\Delta G_U$ is negative and that, therefore, $pK_a^F > pK_a^D$. The overall $\Delta\Delta G_U$ between pH 2 and 7 of ~5 kJ/mol obtained from urea and thermal unfolding can be ascribed to a decrease in the average pK_a of 0.1 pH unit for the 10 side chain carboxyl groups of AB_{SS} (solid line in Figure 6b). The larger change of $\Delta\Delta G_U$ obtained from GdmCl unfolding can be ascribed to a mean pK_a decrease of 0.3 pH unit (dotted line in Figure 6b). Calculation of the pK_a shifts is based on the relationship

$$\Delta\Delta G_U = -2.303RT\Delta\nu \quad (12)$$

where $\Delta\nu$ is the difference in the number of protons bound to the Glu side chains in the folded and denatured state, respectively. The change of $\Delta\nu$ with pH was numerically integrated from $\Delta\nu = \delta\Delta pK_U/\delta pH$.

As a control, we have also calculated the pH−stability profile from the data in Figure 3 using the relationship between $\Delta\nu$, ΔH_m, and T_m:

$$\Delta\nu = \frac{d(\ln K_U)}{d[H^+]} = \frac{1}{2.303}\frac{d(\ln K_U)}{dT}\frac{dT_m}{dpH} = \frac{1}{2.303}\frac{\Delta H_U}{RT_m^2}\frac{dT_m}{dpH} \quad (13)$$

The result of this calculation is shown as empty circles in Figure 6b. The data approximately fit the experimental pH−stability curve from the urea and thermal unfolding experiments. This clearly indicates that the larger stability change seen in GdmCl unfolding (and the larger apparent pK_a shift between the folded and denatured states) must by caused by a peculiarity of GdmCl, which can screen charge−charge interactions (*5*, *60*−*63*).

DISCUSSION

pH-Dependent Stability of Coiled Coils. Salt bridges between the helices of a coiled coil were postulated long ago (*25*), yet their energetic contribution to stability has been controversial ever since. One reason is that the stability of many natural and synthetic coiled coils is pH-independent, or even slightly increasing at acidic pH, and that the change in stability with ionic strength is small (*18*, *20*, *40*, *64*−*68*). If ion pairs were stabilizing, coiled coils should be less stable when the side chain carboxylates are protonated; hence, stability should be lower at acidic pH. This is rarely seen. A small decrease in stability at acidic pH has been reported for a coiled coil featuring many inter- and intrahelical salt bridges at very low, nonphysiological ionic strengths but not under more "natural" conditions of 0.1−0.2 M salt (*58*, *69*).

Thermodynamics of Salt Bridges. From a thermodynamic point of view, the difference in pK_a between the folded and unfolded states provides a direct, model-independent measure of the contribution of an ionizable group to the free energy of folding (*44*). Equation 11 states that the pK_a of the side chain carboxyl group of Glu is lower when it is part of a stabilizing salt bridge, i.e., when $pK_a^F - pK_a^D < 0$. A classic example of stabilizing salt bridges is the catalytic triad of chymotrypsin; a dramatic example is the buried salt bridge in T4 lysozyme (*70*).

Our previous NMR titration experiments have shown that, compared to a pK_a of 4.2−4.4 for a freely accessible residue, none of the six Glu residues involved in salt bridges has a suspiciously low pK_a, perhaps excluding Glu-15 (Table 1). On the contrary, some pK_a values are surprisingly high, and

the mean pK_a of all six Glu residues involved in salt bridges is 4.48. This has tempted us to speculate that, overall, the salt bridges of AB_{SS} are destabilizing the coiled coil conformation, which we now have confirmed with the pH−stability profiles shown in Figure 6.

There are several contributions to the overall free energy change resulting from the formation of a salt bridge. One way of partitioning $\Delta G_U^{\text{salt bridge}}$ is as follows (*44*)

$$\Delta G_U^{\text{salt bridge}} = \Delta G_U^{\text{Coul}} + \Delta G_U^{\text{desolv}} + \Delta G_U^{\text{conf}} + \Delta G_U^{\text{other}} \quad (14)$$

ΔG_U^{Coul} is the Coulombic attraction or repulsion between the charges, $\Delta G_U^{\text{desolv}}$ is the free energy difference due to desolvation of the free charges that form the salt bridge, ΔG_U^{conf} is the change in free energy caused by fixing the charges of the salt bridge, and $\Delta G_U^{\text{other}}$ summarizes all other energetic contributions to $\Delta G_U^{\text{salt bridge}}$. Only the Coulombic attraction always contributes favorably to the stability of the salt bridge. However, ΔG_U^{Coul} is highly variable. It depends on the distance between the charges and their reciprocal orientation, and it is proportional to the inverse of the dielectric constant. Thus, ΔG_U^{Coul} is particularly large for a salt bridge in the interior of a protein, as in the case of the Asp−His salt bridge in T4 lysozyme for which the pK_a of Asp is 0.5 instead of the usual 3.5−4 (*70*). The ΔG_U^{Coul} of a salt bridge exposed to the aqueous environment on the surface of a protein is typically small.

$\Delta G_U^{\text{desolv}}$ is energetically unfavorable and depends on the degree of exposure of the salt bridge. It may be small for a surface-exposed salt bridge and large for a salt bridge in the protein interior. ΔG_U^{conf} is entropically unfavorable since it originates mainly from freezing of the side chains in a particular conformation. $\Delta G_U^{\text{other}}$ includes contacts of the salt bridge with neighboring residues, changes in solvent entropy around the salt bridge, interactions with other full or partial charges of the molecule such as other charged side chains or helix dipoles, etc. In summary, the contribution of $\Delta G_U^{\text{salt bridge}}$ to protein stability is governed by the favorable term ΔG_U^{Coul} as much as by the mostly unfavorable terms ΔG_U^{conf} and $\Delta G_U^{\text{desolv}}$ and the difficult to predict value of $\Delta G_U^{\text{other}}$. Unfortunately, one often has in mind ΔG_U^{Coul} alone when considering the energetic contribution of a salt bridge to protein stability. In other words, one tends to forget that $\Delta G_U^{\text{salt bridge}}$ depends on a delicate balance of forces so that a small shift can take the stability contribution of a salt bridge either way.

Why Is AB_{SS} More Stable at Acidic pH? Geometrical constraints greatly influence the strength of a salt bridge (*3*, *4*, *7*, *71*). In the case of a leucine zipper, computational analysis of the c-Myc-Max leucine zipper revealed wide variation in the energetics of interhelical ion pairs among 40 energy-minimized NMR structures, and the variation was assigned to widely differing geometries of the ion pairs (*71*). A similar heterogeneity of ion pair geometry is seen among AB_{SS} structures (Figure 1c and ref *33*). The variation becomes even larger in multiple molecular dynamics simulations (*52*). Thus, the highly variable geometry of a salt bridge is one reason, overall, $\Delta G_U^{\text{salt bridge}}$ may be negative so that protonation of the Glu side chain stabilizes the coiled coil conformation.

There is a second important reason the protonated Glu can be more stabilizing in a leucine zipper. The hydrophobic core of a coiled coil is formed by the side chains in the *a* and *d* positions to which the side chains in positions *e* and *g* are adjacent. Residues in positions *g* and *e* have been characterized as half-buried and have been given a dual role of forming hydrophobic and polar interactions (*26*). The polar end of an *e* or *g* side chain is exposed to the aqueous environment, and the rest of the side chain forms part of the coiled coil interface. Indeed, the *g* and *e* residues of AB_{SS} are 50−60% exposed to the aqueous environment, the *a* and *d* residues 10−20%, and the *a*, *b*, and *f* residues >80% (*33*). The protonated Glu side chain is considerably less polar than the charged side chain. It has the character of an almost-hydrophobic residue. Therefore, it can better contribute to hydrophobic packing. The side chains in the *e* and *g* positions can fold back and oppose the hydrophobic side chains in the *d* and *a* positions as seen in the NMR structures of AB_{SS} at low pH (*33*). Strengthening of the hydrophobic core is indicated by a higher degree of helicity at acidic pH revealed by a more negative $[\theta]_{222}$ at pH 2 (Figure 5). Indeed, a leucine zipper with all Glu residues in positions *e* and *g* is very stable and folds at a diffusion-limited rate below pH 3 (*72*). In terms of eq 14, protonation of Glu means that the favorable ΔG_U^{Coul} is lost but at least partly compensated by a favorable contribution to $\Delta G_U^{\text{other}}$ due to an increased level of hydrophobic packing. In addition, $\Delta G_U^{\text{desolv}}$ and ΔG_U^{conf} are likely to be less unfavorable since there is less desolvation cost and probably less entropic penalty when no salt bridge is formed.

In conclusion, two aspects can make interhelical salt bridges in leucine zippers energetically unfavorable: the often far from optimized geometries and charge−charge distances of the salt bridges and the contribution of the protonated Glu side chains to the hydrophobic core.

Denaturant-Dependent Free Energy Changes. The pH−stability curve of AB_{SS} is steeper when calculated from the GdmCl unfolding data (Figure 6). Discrepant results from urea and GdmCl unfolding are well-known (*5*, *60*−*63*). The difficulty is that in the linear extrapolation model, the properties of the folded and denatured state in the transition zone of unfolding, that is, in the presence of sometimes high concentrations of denaturant, are projected to zero denaturant concentration. If the denaturant alters the thermodynamic character of the folded and denatured states, extrapolation to zero denaturant concentration may not yield the same free energy of unfolding as thermal unfolding (*5*). Hence, if urea and GdmCl affect the structural nature of AB_{SS} in different ways, different pH−stability curves result. GdmCl acts as a dissociated salt and screens electrostatic interactions (*5*, *60*, *62*, *63*). Monera and co-workers were the first to show a strong electrostatic screening effect of GdmCl, but not of urea, on coiled coils (*60*). Hence, the lower stability of folded AB_{SS} at neutral pH in GdmCl unfolding (ΔG_U = 13 kJ/mol as compared to ΔG_U = 17 kJ/mol for urea unfolding; Figure 6a) could be due to a smaller value of ΔG_U^{Coul} caused by charge screening above pH 4. At low pH, however, AB_{SS} has a net charge of +12 and there is charge−charge repulsion in the folded conformation of AB_{SS}. In terms of eq 14, $\Delta G_U^{\text{other}}$ will contain an unfavorable component from charge−charge repulsion at acidic pH. GdmCl, but not urea, screens the charge−charge repulsion, increasing ΔG_U (ΔG_U = 29

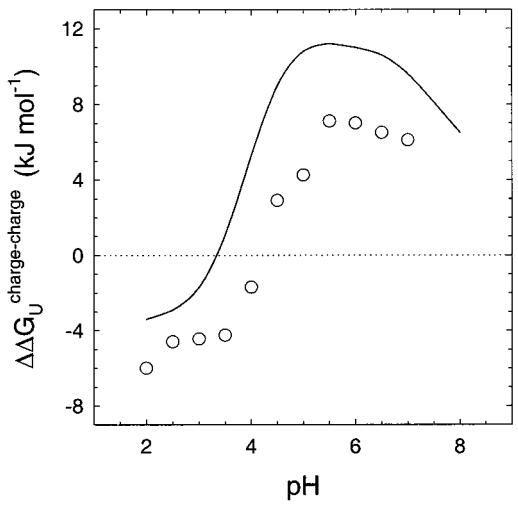

FIGURE 7: Estimated contribution of charge−charge interaction to the free energy change ΔG_U. $\Delta\Delta G_U^{charge-charge}$ was calculated with eq 15 using ΔG_U values from GdmCl unfolding (Figure 6a, circles) and the mean ΔG_U values of urea and heat unfolding (Figure 6a, squares and triangles). The solid line shows values of $\Delta\Delta G_U^{charge-charge}$ calculated with the help of pK_a values for the native and denatured states and setting the desolvation, background interaction, and conformational terms to zero. $\Delta\Delta G_U^{charge-charge}$ corresponds, in principle, to ΔG_U^{Coul} of eq 14. See Materials and Methods for details of this calculation.

kJ/mol, compared to a value of 23 kJ/mol for urea unfolding at pH 2).

If charge−charge interactions are screened by GdmCl but not by urea, one may estimate charge−charge interaction from the following (*5*)

$$\Delta\Delta G_U^{charge-charge} = \Delta G_U^{heat/urea} - \Delta G_U^{GdmCl} \quad (15)$$

A positive $\Delta\Delta G_U^{charge-charge}$ indicates stabilizing charge−charge interactions and a negative $\Delta\Delta G_U^{charge-charge}$ destabilizing charge−charge interactions. $\Delta G_U^{heat/urea}$ is ΔG_U from heat or urea unfolding, and ΔG_U^{GdmCl} is ΔG_U from GdmCl unfolding. Figure 7 shows the change in $\Delta\Delta G_U^{charge-charge}$ with pH. The profile is in agreement with our interpretation of charge screening by GdmCl above and below pH 4. Charge−charge interactions stabilize AB_{SS} when the Glu side chains are deprotonated and the net charge of AB_{SS} approaches zero. At low pH, charge−charge interactions are destabilizing because of the large positive charge of the zipper.

We have also attempted to compute the effect of charge−charge interactions with the help of pK_a values calculated for the native and denatured states and setting the desolvation and background interaction terms to zero. The resulting curve for $\Delta\Delta G_U^{charge-charge}$, shown as a continuous line in Figure 7, is in fair agreement with the experimental values of $\Delta\Delta G_U^{charge-charge}$ calculated by eq 15.

Calculation of the pH−Stability Curve Using a Simple Model of the Unfolded State. The above considerations are focused exclusively on the folded state of AB_{SS}. However, heat and denaturant also influence the ensemble of denatured states, leading to other plausible interpretations of the pH−stability profile. We have tried to calculate a pH−stability curve using the experimental pK_a values of folded AB_{SS} (Table 1) and the pK_a values calculated for a simple model of the unfolded state (*51*). In the model, the important contributions to the pK_a values arise from charge−charge interactions between sequentially adjacent residues in the unfolded peptide chain. Applied to the AB_{SS} zipper, the model predicts a mean pK_a of 4.22 for the 10 Glu side chains of the unfolded protein. The downshift of the mean pK_a is mainly caused by electrostatic interactions in the denatured peptide chain between neighboring residues E6, K7, and E8, and E27, H28, and E29. The resulting pH−stability curve, shown as a dashed line in Figure 6b, lies below the curve from urea and/or heat unfolding and slightly to the right of the curve from GdmCl unfolding. We find this to be a surprisingly good correspondence with experiment in view of the very simple assumptions on which the model is based. Most importantly, the calculation demonstrates that the lower stability of AB_{SS} above pH 4 could also be explained, at least in part, by a higher stability of the ensemble of denatured states.

Are Destabilizing Salt Bridges at Variance with Mutational Studies on Leucine Zippers? The results presented here seem to contradict several mutational studies (*19*, *20*, *24*, *40*, *73*). Removing charges in the *e* and *g* positions by mutation (Glu → Ala, Lys → Ala, and Arg → Ala) was reported to destabilize the coiled coil by 1−2 kJ/mol per lost salt bridge (*19*, *24*, *40*). The interpretation of mutational effects can be difficult (*74*), but great care has been taken by Vinson and co-workers to rule out nonspecific mutational effects with the help of double-mutation cycles (*19*, *24*). As a result, it was concluded that the coupling energy of a salt bridge (corresponding to $\Delta G_U^{salt\ bridge}$) has a favorable electrostatic component (ΔG_U^{Coul}). This makes sense and does not contradict the finding that a salt bridge can destabilize the folded coiled coil. Destroying a salt bridge by protonation of Glu and destroying a salt bridge by removal of Glu through mutation are different sides of a coin. When the Glu side chain is protonated, stabilization follows in a thermodynamically stringent way if the side chain's pK_a is higher in the folded than in the unfolded zipper (B → A transition in Figure 8). The reason for the higher stability of structure A has been discussed above: gain in hydrophobic interaction and perhaps less desolvation and lower conformational costs. In contrast, when the charge is removed by mutation (B → C transition in Figure 8), Coulombic attraction is lost and not compensated by a gain from new interactions. Overall, the stability increases in the C → B → A direction. In other words, mutation C is destabilizing with respect to B, but B is destabilizing with respect to A. Since, however, the amount of A is negligible at neutral pH, mutation truly indicates stabilization by the salt bridge at neutral pH.

Why Are Interhelical Salt Bridges Frequent in Natural Coiled Coils? If $\Delta G_U^{salt\ bridge}$ is negative and reduces the free energy of unfolding of the coiled coil, one would not expect Glu, Lys, and Arg so frequently to be in the *e* and *g* positions of natural coiled coils (*25*, *75*). We believe the main reason is that among the 20 amino acid residues in proteins, Glu, Gln, Lys, and Arg are best suited for the dual role of forming hydrophobic and polar interactions.[7] The side chains of the other polar residues (Ser, Thr, Asp, and Asn) are too short to contribute significantly to the hydrophobic core. Furthermore, if there is Glu in one helix, Lys or Arg in the opposite

[7] Statistical distribution of residues in the *e* and *g* positions of coiled coils: 26% Glu, 21% Lys and Arg, and 14% Gln (*75*).

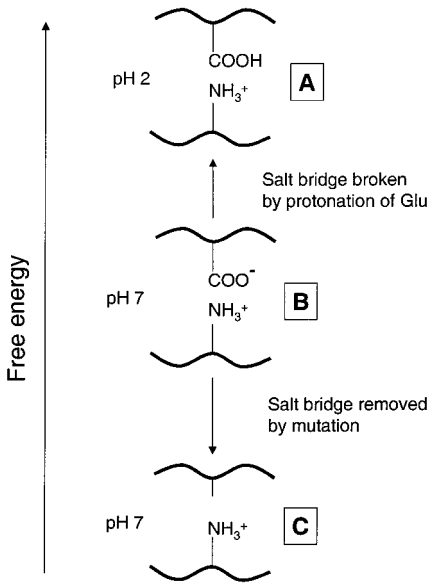

$$\Delta G_U^{\text{salt bridge}} = \Delta G_U^{\text{Coul}} + \Delta G_U^{\text{desolv}} + \Delta G_U^{\text{conf}} + \Delta G_U^{\text{other}}$$

FIGURE 8: Thermodynamics of salt bridges in leucine zippers. The scheme explains why mutational studies are not at variance with the conclusion of the study presented here. At neutral pH, removal of a salt bridge by mutation can destabilize the coiled coil conformation (B → C) even if protonation of the same salt bridge is stabilizing (B → A). The reason is that the free energy of unfolding of a salt bridge, $\Delta G_U^{\text{salt bridge}}$, depends on a delicate balance of favorable and unfavorable forces. See the text for a detailed discussion.

helix prevents charge−charge repulsion; hence, opposite charges (attraction) are preferred over like charges (repulsion). Nevertheless, the occurrence of oppositely charged residues in the *g* and *e* positions is by far not exclusive. Hence, it is not surprising that interhelical ion pairs were not maximized in the most stable heterodimeric leucine zippers selected from an in vivo library in which the *e* and *g* positions were randomized to Gln, Glu, Arg, and Lys (*76*). Paradoxically, interhelical salt bridges are preferred because they contribute to the hydrophobic core of the coiled coil. This proposal may be tested by mutating the basic residue of a salt bridge to a hydrophobic residue. This will decrease stability at neutral pH by removing the salt bridge. But at acidic pH, the mutant should be more stable than the wild type because the hydrophobic core is further strengthened by the hydrophobic residue juxtaposed to the protonated Glu.

CONCLUSION

The heterodimeric leucine zipper AB_{SS} can form seven interhelical salt bridges, of which six are seen in the NMR structures. Their protonation leads to net stabilization of the coiled coil conformation, in agreement with high pK_a values of several Glu side chains in the folded zipper (*33*). Therefore, the salt bridges are, on average, destabilizing the coiled coil when compared to the protonated form. The main reason is that the contribution of a salt bridge to the stability of a coiled coil is a delicate balance between favorable and unfavorable energetic contributions. In the case of the designed leucine zipper AB_{SS}, unfavorable contributions dominate. This will be true also for many other leucine zippers. The finding is not in conflict with mutational studies which mostly indicate that salt bridges stabilize the coiled coil conformation at neutral pH. Destroying a salt bridge by protonating Glu can stabilize the hydrophobic core of the zipper, thereby compensating for the loss of Coulombic attraction. Removing a salt bridge by mutation eliminates Coulombic attraction without compensation from new interactions.

SUPPORTING INFORMATION AVAILABLE

Figure and table of T_m and ΔH_m values in the presence of nondenaturing amounts of GdmCl and urea, respectively; table of T_m and ΔH_m values of thermal unfolding; and tables of ΔG_U and *m* values for denaturant unfolding. This material is available free of charge via the Internet at http://pubs.acs.org.

REFERENCES

1. Perutz, M. F. (1978) *Science 201*, 1187−1191.
2. Hendsch, Z. S., and Tidor, B. (1994) *Protein Sci. 3*, 211−226.
3. Xiao, L., and Honig, B. (1999) *J. Mol. Biol. 289*, 1435−1444.
4. Kumar, S., and Nussinov, R. (1999) *J. Mol. Biol. 293*, 1241−1255.
5. Ibarra-Molero, B., Loladze, V. V., Makhatadze, G. I., and Sanchez-Ruiz, J. M. (1999) *Biochemistry 38*, 8138−8149.
6. Strop, P., and Mayo, S. L. (2000) *Biochemistry 39*, 1251−1255.
7. Kajander, T., Kahn, P. C., Passila, S. H., Cohen, D. C., Lethiö, L., Adolfsen, W., Warwicker, J., Schell, U., and Goldman, A. (2000) *Structure 8*, 1203−1214.
8. Miller, S., Janin, J., Lesk, A. M., and Chothia, C. (1987) *J. Mol. Biol. 196*, 641−656.
9. Eisenberg, D., and McLachlan, A. D. (1986) *Nature 319*, 199−203.
10. Crick, F. H. C. (1953) *Acta Crystallogr. 6*, 689−697.
11. Lupas, A. (1996) *Trends Biochem. Sci. 21*, 375−382.
12. Hope, I. A., and Struhl, K. (1987) *EMBO J. 6*, 2781−2784.
13. Landschulz, W. H., Johnson, P. F., and McKnight, S. L. (1988) *Science 240*, 1759−1764.
14. Hurst, H. C. (1996) *Leucine Zippers: Transcription factors*, 3rd ed., Academic Press, London.
15. Alber, T. (1992) *Curr. Opin. Genet. Dev. 2*, 205−210.
16. Vinson, C. R., Hai, T., and Boyd, S. M. (1993) *Genes Dev. 7*, 1047−1058.
17. Graddis, T. J., Myszka, D. G., and Chaiken, I. M. (1993) *Biochemistry 32*, 12664−12671.
18. O'Shea, E. K., Lumb, K. J., and Kim, P. S. (1993) *Curr. Biol. 3*, 658−667.
19. Krylov, D., Mikhailenko, I., and Vinson, C. (1994) *EMBO J. 13*, 2849−2861.
20. Zhou, N. E., Kay, C. M., and Hodges, R. S. (1994) *J. Mol. Biol. 237*, 500−512.
21. Kohn, W. D., Monera, O. D., Kay, C. M., and Hodges, R. S. (1995) *J. Biol. Chem. 270*, 25495−25506.
22. Jelesarov, I., and Bosshard, H. R. (1996) *J. Mol. Biol. 263*, 344−358.
23. Kohn, W. D., Kay, C. M., and Hodges, R. S. (1997) *J. Mol. Biol. 267*, 1039−1052.
24. Krylov, D., Barchi, J., and Vinson, C. (1998) *J. Mol. Biol. 279*, 959−972.
25. McLachlan, A. D., and Stewart, M. (1975) *J. Mol. Biol. 98*, 293−304.
26. O'Shea, E. K., Klemm, J. D., Kim, P. S., and Alber, T. (1991) *Science 254*, 539−544.
27. Ellenberger, T. (1994) *Curr. Opin. Struct. Biol. 4*, 12−21.
28. O'Shea, E. K., Rutkowski, R., Stafford, W. F., III, and Kim, P. S. (1989) *Science 245*, 646−648.
29. Lamb, P., and McKnight, S. L. (1991) *Trends Biochem. Sci. 16*, 417−422.
30. Baxevanis, A. D., and Vinson, C. R. (1993) *Curr. Opin. Genet. Dev. 3*, 278−285.

31. O'Shea, E. K., Rutkowski, R., and Kim, P. S. (1992) *Cell 68*, 699−708.
32. Lavigne, P., Crump, M. P., Gagne, S. M., Hodges, R. S., Kay, C. M., and Sykes, B. D. (1998) *J. Mol. Chem. 281*, 165−181.
33. Marti, D. N., Jelesarov, I., and Bosshard, H. R. (2000) *Biochemistry 39*, 12804−12818.
34. Lumb, K. J., and Kim, P. S. (1995) *Science 268*, 436−439.
35. Lumb, K. J., and Kim, P. S. (1996) *Science 271*, 1137−1138.
36. Lavigne, P., Kondejewski, L. H., Houston, M. E., Jr., Sönnichsen, F. D., Lix, B., Sykes, B. D., Hodges, R. S., and Kay, C. M. (1995) *J. Mol. Biol. 254*, 505−520.
37. Lavigne, P., Sönnichsen, F. D., Kay, C. M., and Hodges, R. S. (1996) *Science 271*, 1136−1137.
38. Wendt, H., Leder, L., Härmä, H., Jelesarov, I., Baici, A., and Bosshard, H. R. (1997) *Biochemistry 36*, 204−213.
39. Myszka, D. G., and Chaiken, I. M. (1994) *Biochemistry 33*, 2363−2372.
40. Zhou, N. E., Kay, C. M., and Hodges, R. S. (1994) *Protein Eng. 7*, 1365−1372.
41. Nozaki, Y., and Tanford, C. (1967) *Methods Enzymol. 11*, 715−734.
42. Richartz, R., and Wüthrich, K. (1978) *Biopolymers 17*, 2133−2141.
43. Dames, S. A., Kammerer, R. A., Moskau, D., Engel, J., and Alexandrescu, A. T. (1999) *FEBS Lett. 446*, 75−80.
44. Yang, A. S., and Honig, B. (1994) *J. Mol. Biol. 237*, 602−614.
45. Edelhoch, H. (1967) *Biochemistry 6*, 1948−1954.
46. Gill, S. C., and von Hippel, P. (1989) *Anal. Biochem. 182*, 319−326.
47. Pace, C. N. (1986) *Methods Enzymol. 131*, 266−280.
48. Tanford, C. (1970) *Adv. Protein Chem. 24*, 1−95.
49. Makhatadze, G. I., and Privalov, P. L. (1992) *J. Mol. Biol. 226*, 491−505.
50. Jelesarov, I., and Bosshard, H. R. (1999) *J. Mol. Recognit. 12*, 13−18.
51. Warwicker, J. (1999) *Protein Sci. 8*, 418−425.
52. Gorfe, A. A., Ferrara, P., Caflisch, A., Marti, D. N., Bosshard, H. R., and Jelesarov, I. (2001) *Proteins* (in press).
53. Schaefer, M., Sommer, M., and Karplus, M. (1997) *J. Phys. Chem. B 101*, 1663−1683.
54. Bashford, D., and Gerwert, K. (1992) *J. Mol. Biol. 224*, 473−486.
55. Bashford, D. (1997) in *Volume 1343 of Lecture Notes in Computer Science* (Ishikawa, Y., Oldehoeft, R. R., Reynders, J. V. W., and Tholburn, M., Eds.) pp 223−240, Springer, Berlin.
56. Sitkoff, D., Sharp, K. A., and Honig, B. (1994) *Biophys. Chem. 51*, 397−403.
57. Scholtz, J. M., Qian, H., Robbins, V. H., and Baldwin, R. L. (1993) *Biochemistry 32*, 9668−9676.
58. Yu, Y. H., Monera, O. D., Hodges, R. S., and Privalov, P. L. (1996) *Biophys. Chem. 59*, 299−314.
59. Luo, P., and Baldwin, R. L. (1997) *Biochemistry 36*, 8413−8421.
60. Monera, O. D., Kay, C. M., and Hodges, R. S. (1994) *Protein Sci. 3*, 1984−1991.
61. Gupta, R., Yadav, S., and Ahmad, F. (1996) *Biochemistry 35*, 11925−11930.
62. Bolen, D. W., and Yang, M. (2000) *Biochemistry 39*, 15208−15216.
63. Yang, M., Ferreon, A. C. M., and Bolen, D. W. (2000) *Proteins: Struct., Funct., Genet. 4*, 44−49.
64. Lowey, S. (1965) *J. Biol. Chem. 240*, 2421−2427.
65. Woods, E. F. (1969) *Int. J. Protein Res. 1*, 29−43.
66. Lau, S. Y. M., Taneja, A. K., and Hodges, R. S. (1984) *J. Biol. Chem. 259*, 13253−13261.
67. Hodges, R. S., Semchuk, P. D., Taneja, A. K., Kay, C. M., Parker, J. M. R., and Mant, C. T. (1988) *Pept. Res. 1*, 19−30.
68. Zhou, N. E., Zhu, B.-Y., Kay, C. M., and Hodges, R. S. (1992) *Biopolymers 32*, 419−426.
69. Yu, Y. H., Monera, O. D., Hodges, R. S., and Privalov, P. L. (1996) *J. Mol. Biol. 255*, 367−372.
70. Anderson, D. E., Becktel, W. J., and Dahlquist, F. W. (1990) *Biochemistry 29*, 2403−2408.
71. Kumar, S., and Nussinov, R. (2000) *Proteins 41*, 485−497.
72. Dürr, E., Jelesarov, I., and Bosshard, H. R. (1999) *Biochemistry 38*, 870−880.
73. Spek, E. J., Bui, A. H., Lu, M., and Kallenbach, N. R. (1998) *Protein Sci. 7*, 2431−2437.
74. Serrano, L., Horovitz, A., Avron, B., Bycroft, M., and Fersht, A. R. (1990) *Biochemistry 29*, 9343−9352.
75. Cohen, C., and Parry, D. A. D. (1990) *Proteins 7*, 1−15.
76. Arndt, K. M., Pelletier, J. N., Muller, K. M., Alber, T., Michnick, S. W., and Plückthun, A. (2000) *J. Mol. Biol. 295*, 627−639.

BI011920C